J Biomol NMR (2013) 55:239–247
DOI 10.1007/s10858-013-9705-2

ARTICLE

Probing non-specific interactions of Ca^{2+}-calmodulin in *E. coli* lysate

Michael P. Latham · Lewis E. Kay

Received: 20 November 2012 / Accepted: 2 January 2013 / Published online: 17 January 2013

Abstract The biological environment in which a protein performs its function is a crowded milieu containing millions of molecules that can potentially lead to a great many transient, non-specific interactions. NMR spectroscopy is especially well suited to study these weak molecular contacts. Here, non-specific interactions between the Ca^{2+}-bound form of calmodulin (CaM) and non-cognate proteins in *Escherichia coli* lysate are explored using Ile, Leu, Val and Met methyl probes. Changes in CaM methyl chemical shifts as a function of added *E. coli* lysate are measured to determine a minimum 'average' dissociation constant for interactions between Ca^{2+}-CaM and *E. coli* lysate proteins. ^{2}H R_2 and ^{13}C R_1 spin relaxation rates report on the binding reaction as well. Our results further highlight the power of methyl containing side-chains for characterizing biomolecular interactions, even in complex *in-cell* like environments.

Keywords Deuterium relaxation · Chemical shift titration · In "cell-like" · Methyl side-chain dynamics · $^{13}CHD_2$ methyl isotopomers

Introduction

The cellular environment is a complex, heterogeneous mixture of molecules, with protein concentrations that can approach 400 g/L (Fulton 1982; Neidhardt 1987). Such high levels of macromolecules lead to greater excluded volume effects and increased viscosity compared to the typical in vitro conditions in which the majority of biochemical and biophysical experiments are performed and, therefore, to changes in protein stability, function, and interactions (Miklos et al. 2010, 2011; Wang et al. 2011). For example, weak, non-specific contacts between proteins might be predicted because of the higher effective *in-cell* protein concentrations (Miklos et al. 2010; Wang et al. 2011).

NMR spectroscopy is particularly well suited for the characterization of transiently formed, relatively low affinity complexes. Since such complexes typically exchange rapidly between bound and free states, changes in peak positions as a function of the addition of one of the binding partners can be quantified to give the dissociation constant, K_D, of the interaction in the classic NMR titration experiment (Campbell and Dwek 1984; Johnson et al. 1996). Other methodologies have been developed for quantifying the kinetics and thermodynamics of binding events that occur in the slow and intermediate exchange time-scale regimes (Ishima and Torchia 2000; Palmer et al. 2001; Zuiderweg 2002; Mittermaier and Kay 2006). The vast majority of such binding experiments have been performed in carefully controlled buffer conditions that greatly simplify the analysis of the data since, for example, concentrations of all of the molecular players can be controlled. Experiments that are performed *in-cell* or under *in-cell* conditions are more difficult to interpret, but recently, NMR spectroscopy has emerged as a powerful technique to study and quantify interactions under these more biological conditions (Serber et al. 2001; Sakai et al. 2006; Selenko et al. 2006; Reckel et al. 2007). Several of these studies have highlighted differences between protein stability and dynamics in a "cell-like" environment versus a dilute aqueous buffer (Li and Pielak 2009; Hong and

M. P. Latham · L. E. Kay (✉)
Departments of Molecular Genetics, Biochemistry and Chemistry, The University of Toronto, Toronto, ON M5S 1A8, Canada
e-mail: kay@pound.med.utoronto.ca

L. E. Kay
Program in Molecular Structure and Function, Hospital for Sick Children, 555 University Avenue, Toronto, ON M5G 1X8, Canada

Gierasch 2010; Miklos et al. 2010, 2011; Wang et al. 2011; Latham and Kay 2012).

We have previously used the protein calmodulin (CaM) as a model system for studying how the cellular environment perturbs picosecond (ps)—millisecond (ms) time-scale protein dynamics (Latham and Kay 2012). Unlike the majority of other such NMR studies that have exploited backbone amide groups as reporters, we prepared highly deuterated, Ileδ1-, Leuδ-, Valγ- and Metε-$^{13}CHD_2$ methyl labeled protein and focused on methyl group probes. An excellent correlation for both the amplitude and the time-scale of methyl containing side-chain dynamics was observed in a complex of CaM and a high affinity peptide from smooth muscle myosin light chain kinase, smMLCK(p) (Ca^{2+}-CaM-smMLCK(p)), dissolved in *E. coli* lysate (100 g/L) and in buffer. In contrast, a similar set of experiments, recorded on lysate and buffer samples of Ca^{2+}-loaded CaM (Ca^{2+}-CaM) showed that ^{1}H and ^{13}C transverse relaxation rates of CaM dissolved in lysate were modulated by an exchange process resulting from interactions with non-cognate *E. coli* proteins. Fast time-scale dynamics were not quantified at that time. In an effort to better understand the observed exchange process we have performed a titration of Ca^{2+}-CaM with *E. coli* lysate. We show that the exchange between bound and free Ca^{2+}-CaM is fast on the NMR chemical shift time-scale and report a lower bound for an 'effective' K_D of the binding event. In addition, we illustrate that transverse ^{2}H spin relaxation rates are a powerful reporter of the non-specific binding events that occur in *E. coli* lysate. Finally, differences between interactions of CaM in non-cognate *E. coli* and cognate yeast lysate environments are clearly 'visualized' in a comparison of methyl ^{13}C-^{1}H correlation spectra.

Materials and methods

Sample preparation

U-[^{2}H,^{15}N], Ileδ1-[$^{13}CHD_2$], Leuδ,Valγ-[$^{13}CHD_2$], Metε-[$^{13}CHD_2$] labeled CaM samples were prepared by over-expression in BL21(DE3) pLysS *E. coli* in deuterated M9 minimal media with ^{2}H, ^{13}C-glucose (3 g/L) and ^{15}N ammonium chloride (1 g/L) as the sole carbon and nitrogen sources, respectively. $^{13}CHD_2$-labeled precursors were added 1 h before protein induction, as described by Tugarinov et al. (Tugarinov et al. 2006). CaM was over-expressed with 1 mM IPTG for ~16 h at 30 °C, purified as described previously (Latham and Kay 2012) and buffer exchanged into 20 mM imidazole, pH 6.5 (uncorrected), 100 mM KCl, 6 mM $CaCl_2$, 100 μM NaN_3 in 100 % D_2O.

Escherichia coli lysate was prepared from BL21(DE3) pLysS cells grown in LB media supplemented with chloramphenicol (34 μg/mL) until an OD_{600} ~0.9 was reached. After the cells were separated from the media they were resuspended in 100 % D_2O and lysed. The insoluble material was removed by centrifugation (39,000×*g*), and 5 mM benzamidine, 0.1 mg/mL PMSF, 100 μM NaN_3 and 6 mM $CaCl_2$ was added to the lysate. The lysate was then filtered through a 0.22 μm syringe filter in order to maximize sample stability. The size of the filter pores is such that all ingredients of the lysate can pass through (MW coutoff $<4 \times 10^9$ Da); by contrast, intact bacteria are eliminated from the lysate. Finally, the resultant filtrate is concentrated in a 3 kDa MWCO Amicon centrifugal concentrator. Total lysate protein concentration was determined via the BCA assay (Pierce).

To quantify the interactions between Ca^{2+}-CaM and non-cognate proteins in *E. coli* lysate, a titration experiment was performed utilizing two 500 μL, 1 mM Ca^{2+}-CaM NMR samples. Initially, the samples comprised Ca^{2+}-CaM in aqueous buffer (sample 1) and Ca^{2+}-CaM in 100 g/L *E. coli* lysate (sample 2). For each point in the titration, equal volume aliquots were removed from each sample and replaced with the aliquot from the other sample, such that the lysate concentration increased for sample 1 and decreased for sample 2, while the Ca^{2+}-CaM concentration remained the same. This procedure was repeated in 5 g/L steps until both samples reached lysate concentrations of 50 g/L total protein, resulting in 22 titration points (the 50 g/L point was recorded using both samples).

NMR spectroscopy and data analysis

NMR spectra were recorded at 18 °C on a 14.1 T Varian INOVA spectrometer equipped with a triple-resonance, z-axis gradient cryogenically cooled probe. 2D ^{13}C–^{1}H HSQC datasets consisted of 72 × 512 complex points and acquisition times of 26.7 and 64 ms in the indirect and direct dimensions, respectively, with a 660 Hz WALTZ-16 ^{2}H-decoupling field (Shaka et al. 1983) applied during the indirect detection period. Four scans were taken for each point with an inter-scan delay of 2.5 s, resulting in an acquisition time of ~25 min/dataset. ^{1}H single-quantum Carr–Purcell–Meiboom–Gill (CPMG) relaxation dispersion experiments (Carr and Purcell 1954; Meiboom and Gill 1958; Baldwin et al. 2010) were recorded as previously described (Latham and Kay 2012). ^{2}H R_2 and ^{13}C R_1 relaxation rates were acquired with previously published pulse sequences (Tugarinov et al. 2005; Tugarinov and Kay 2005). ^{2}H R_2 rates were determined by quantifying peak intensities from 8 parametrically varied relaxation delays between 0.05 and 3 ms, while ^{13}C R_1 rates were measured from 7 spectra recorded with relaxation delays between 0.04 and 2 s. Relaxation data sets consisted of 72 × 512 complex points, acquisition times of 26.7 and 64 ms in the indirect and direct dimensions, respectively and measurement times of ~16 h (~8 h) for the complete ^{2}H R_2 (^{13}C R_1) series.

NMR spectra were processed using the NMRPipe/NMRDraw suite of programs (Delaglio et al. 1995) and

chemical shifts referenced using the residual H_2O signal. For the titration experiment, referencing was verified by comparing peak positions of 100 μM $^{13}CH_3$-acetate, that was added as an internal standard. Ca^2-CaM methyl side-chain ^1H and ^{13}C chemical shifts were determined at each point of the lysate titration by interpolation using CcPNmr analysis software (Vranken et al. 2005). Changes in chemical shifts upon addition of lysate were fitted, as described in the text, to extract per-residue values of $C_{Lys,1/2}$, the concentration of lysate in g/L required for 50 % bound CaM, as well as a minimum value for K_D. Relaxation rates were determined from fitting peak intensities using the nlinLS routine of NMRPipe to a single-exponential decay function, Ae^{-Rt}, with errors determined from the covariance matrix (Press et al. 1992).

Results and discussion

Ca^{2+}-CaM interacts with lysate

We have previously reported a comparative dynamics study of CaM in aqueous buffer and in *E. coli* lysate focusing on methyl group probes of motion (Latham and Kay 2012). Samples of U-[^2H,^{15}N], Ileδ1-[$^{13}CHD_2$], Leuδ,Valγ-[$^{13}CHD_2$], Metε-[$^{13}CHD_2$] labeled CaM were prepared, as described previously and in Materials and Methods, and a series of ^{13}C, ^1H and ^2H spin relaxation experiments performed. Comparative 2D ^{13}C–^1H spectra of Ca^{2+}-CaM-smMLCK(p) (Fig. 1a) showed that the peptide bound form of CaM is relatively inert to lysate, with essentially no changes to chemical shifts. ^{13}C and ^1H CPMG relaxation dispersion profiles that are sensitive to ms time-scale exchange events, were recorded on samples of Ca^{2+}-CaM-smMLCK(p) in buffer and lysate (referred to as buffer Ca^{2+}-CaM-smMLCK(p) and lysate Ca^{2+}-CaM-smMLCK(p), respectively). Relatively flat dispersion profiles were obtained for all residues (compare orange and blue, Fig. 1b), with curves from the lysate offset relative to those from buffer that reflects a difference in viscosity and hence intrinsic transverse relaxation rates in the two solvents. By contrast, very significant differences in many peak positions were noted in spectra of lysate Ca^{2+}-CaM relative to buffer Ca^{2+}-CaM, Fig. 1c. Linewidths of methyl correlations were also substantially larger in the lysate, reflecting a ms time-scale exchange process, Fig. 1b (compare green and red). Because these dispersions are quenched upon addition of the high affinity peptide smMLCK(p), the exchange was assigned to binding events involving *E. coli* lysate peptides/proteins or potentially even smaller metabolites. These are non-specific interactions in the sense that they arise from weak, transient associations between eukaryotic Ca^{2+}-CaM and non-cognate partners from *E. coli* lysate, localizing to the same binding site as for higher affinity, native interactions such as involving the smMLCK(p) peptide.

A Ca^{2+}-CaM, lysate binding isotherm

In an effort to quantify the non-cognate interactions further, we have carried out a titration whereby increasing amounts of lysate are added to a solution of Ca^{2+}-CaM, with the concentration of CaM kept fixed, as summarized in Materials and Methods. As described above, *E. coli* lysate is a complex mixture consisting of a large number of potential CaM binding targets, and while the concentration of lysate (g/L) is known for each addition of titrant, the concentration of binding competent peptides/proteins is not. In what follows we interpret our data using a simplified and necessarily incomplete binding model,

$$CaM + L \rightleftarrows CaM - L \tag{1}$$

where L refers to a CaM binding partner from the lysate. In the case of exchange that is fast on the NMR chemical shift time-scale (see below) the chemical shift of a methyl probe after addition of aliquot i of the titrant, δ_i, can be expressed as (Johnson et al. 1996)

$$\Delta_i = \delta_i - \delta_F = f_{B,i}(\delta_B - \delta_F) \tag{2}$$

where $\delta_F(\delta_B)$ is the methyl shift in the free(ligand bound) state and $f_{B,i}$ is the mole fraction of CaM that is bound to L,

$$f_{B,i} = \frac{\alpha C_{Lys,i} + [CaM]_T + K_D - \sqrt{(\alpha C_{Lys,i} + [CaM]_T + K_D)^2 - 4[CaM]_T \alpha C_{Lys,i}}}{2[CaM]_T}. \tag{3}$$

In Eq. (3) $C_{Lys,i}$ is the total concentration of added lysate (g/L) at each aliquot i, $[CaM]_T$ is the total concentration of CaM in the sample (in molar) and α is defined as

$$\alpha = \frac{w}{<MW>} \tag{4}$$

where w is the weight fraction of CaM binding competent ligand in the lysate and $<MW>$ is the 'average' molecular weight of a ligand. It follows therefore that $\alpha C_{Lys,i}$ is the total concentration of binding competent ligand (molar) in the NMR sample. In principle, fits of chemical shift

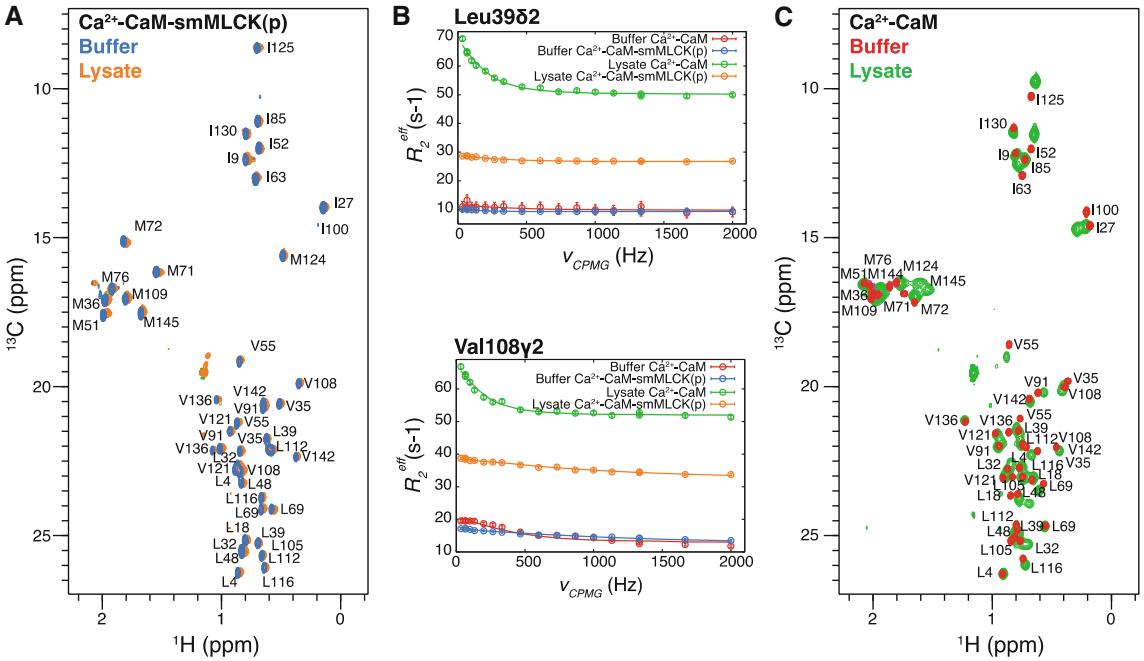

Fig. 1 **a** Methyl ^{13}C–^{1}H correlation spectra of Ca^{2+}-CaM-smMLCK(p) dissolved in buffer (*blue*) or 100 g/L *E. coli* lysate (*orange*). **b** Representative ^{1}H single-quantum CPMG relaxation dispersion profiles for Leu39δ2, Val108γ2 of Ca^{2+}-CaM or Ca^{2+}-CaM-smMLCK(p) dissolved in buffer or lysate, 18 °C, 14.1 T. Colors of the dispersion profiles follow **a** and **c**. The solid lines result from global fitting to a two-site exchange process. **c** Methyl ^{13}C–^{1}H correlation spectra of Ca^{2+}-CaM dissolved in buffer (*red*) or 100 g/L *E. coli* lysate (*green*). **a** and **c** Spectra were recorded at 14.1 T, 18 °C with a previously described pulse sequence for measuring ^{2}H R_2 relaxation rates with $T = 0$ (Tugarinov et al. 2005)

titration profiles (Δ vs C_{Lys}) to Eq. (2) allow extraction of best fit α and K_D values.

Figure 2a highlights a number of regions from ^{13}C–^{1}H HSQC spectra that were recorded as a function of C_{Lys} showing the 'migration' of peaks with added ligand (red to blue). Of note, all of the 34 peaks that could be quantified moved on straight lines, as those shown in the Figure, consistent with a fast exchange process. In addition, values of populations and chemical shift differences, as obtained in fits of CPMG relaxation dispersion profiles recorded on Ca^{2+}-CaM samples at intermediate stages of the titration were highly correlated, that is expected in the fast exchange regime (data not shown).

While the assumption of fast exchange appears to be reasonable (see also below), assuming a single exchange process is almost certainly an oversimplification. We have therefore fit each titration curve to a separate isotherm to extract (α, K_D) values. Notably, α and K_D are correlated. That this is the case can be readily seen in a plot of fitting residual (χ^2) as a function of K_D, for a range of α values in the vicinity of the best-fit parameters (see "Appendix"). Interestingly, while unique values of (α, K_D) cannot be extracted from fits, it is shown in the Appendix that the (α, K_D) pairs that are obtained describe a linear relation that is well approximated by

$$K_D = \alpha C_{Lys,1/2} - 0.5[CaM]_T \quad (5)$$

where $C_{Lys,1/2}$ is the value of C_{Lys} for which $f_B = 0.5$ (i.e., the concentration of lysate in g/L for which 50 % of CaM is in the bound form). Note that Eq. (5) can be derived from Eq. (3) by setting $f_B = 0.5$ and solving for the relation between α and K_D. Robust measures for $C_{Lys,1/2}$ can thus be obtained from fits of the data. In addition, we have also established that despite the cross-talk between fitted (α, K_D), a trimmed 'average' minimum value for K_D, $K_{D,min}$ $\sim$0.22 mM can be estimated for the *E. coli* lysate—Ca^{2+}-CaM interaction (generated by excluding values outside $\pm$ two times the standard deviation of the mean; $K_{D,min}$ values ranging between 0.06 and 0.90 mM for the 34 independent titration curves were obtained, see "Appendix").

Figure 2b shows fits of ^{13}C titration profiles to Eq. (2) for two typical residues, Ile52δ1 and Val108γ2 (corresponding ^{1}H curves are insets) along with extracted $C_{Lys,1/2}$ values. A histogram of the distribution of $C_{Lys,1/2}$ is presented in Fig. 2c; the average value obtained for $<C_{Lys,1/2}>$, 26 g/L, translates into 1.63 mg *E. coli* lysate/mg of CaM to achieve a half bound state. We have also fit the titration data using a fixed value of α for all residues (given by the average over extracted values when both α, K_D were fitting parameters) and obtained a similar $<C_{Lys,1/2}>$ value and distribution as before, $<C_{Lys,1/2}>$ = 31 g/L $\pm$ 12 g/L (all data) and 29 g/L $\pm$ 8 g/L (omitting 3 residues with $C_{Lys,1/2}$

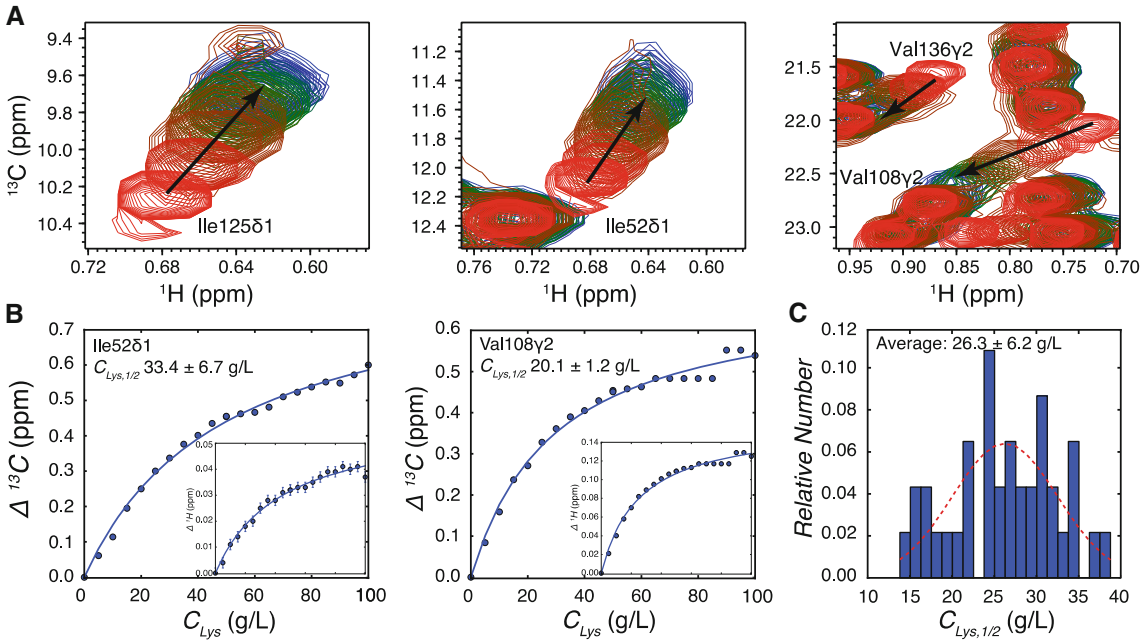

Fig. 2 **a** Selected regions of methyl ^{13}C–^{1}H correlation spectra recorded with different C_{Lys} ranging from 0 to 100 g/L. Steps of 10 g/L are shown from *red* to *blue* and *arrows* denote the linear movement of the peaks with increasing lysate concentration. **b** Representative fits of ^{13}C titration profiles to Eq. (2) with fits of ^{1}H titrations shown in the insets. The fitted $C_{Lys,1/2}$ values are given in the upper left hand corner. **c** Histogram of $C_{Lys,1/2}$ values. The best-fit Gaussian function to the distribution is represented by the *red dashed line*

larger than the mean by more than twice the standard deviation). The relatively small range of per-residue fitted $C_{Lys,1/2}$ values is consistent with the various non-cognate *E. coli* binding partners having similar affinities for CaM. Nevertheless, significant improvements in fits are obtained when each residue is treated independently, as opposed to fixing both α, K_D as global parameters, consistent with a variety of different binding partners, each with a somewhat different affinity.

^{2}H and ^{13}C spin relaxation probes of binding

In an effort to evaluate the sensitivity of ps-ns time-scale dynamics to the binding process, we have recorded ^{2}H R_2 spin relaxation rates of Ca^{2+}-CaM dissolved in 100 g/L lysate and compared these values with those obtained from measurements recorded on a sample in buffer. As described previously, the advantage of using the deuteron as a probe of fast time-scale dynamics is that ^{2}H R_2 values are essentially immune to the effects of chemical exchange, unlike ^{13}C or ^{1}H rates. This results from the fact that (1) ^{2}H relaxation is dominated by the quadrupolar interaction with ^{2}H R_2 values on the order of 300/s, on average, for the Ca^{2+}-CaM sample considered here (i.e., much larger than chemical exchange contributions to transverse relaxation) (Muhandiram et al. 1995) and (2) the small γ of the deuteron attenuates the effects of exchange, since smaller shift changes between exchanging states are observed.

Figure 3a plots ^{2}H R_2 values for Ca^{2+}-CaM dissolved in buffer (y-axis) versus 100 g/L lysate (x-axis). On the basis of the titration data (Fig. 2) we estimate that f_B is close to 1 ($f_B = 0.85 \pm 0.05$) for the lysate sample. For proteins the size of CaM, methyl ^{2}H R_2 values report primarily on the product $S^2\tau_C$ (Tugarinov et al. 2005), where S^2 is the square of the order parameter describing the amplitude of motion of the methyl threefold axis and τ_C is the assumed isotropic correlation time: at 18 °C $\tau_C \sim 15$ ns for CaM in buffer and ~ 2.5 fold larger in lysate (Latham and Kay 2012). The rather poor correlation obtained (Pearson's correlation coefficient of 0.7) reflects both changes in dynamics between bound (lysate) and free (buffer) states (S^2) as well as potentially structural changes that may accompany the binding of non-cognate *E. coli* peptides/proteins (τ_C). It has been shown that the binding of high affinity cognate peptides to CaM ($K_D \sim 1$ nM (Ikura et al. 1992; Lee et al. 2000)) causes very significant structural rearrangements (Ikura et al. 1992; Siivari et al. 1995; Hoeflich and Ikura 2002); whether such changes accompany the much lower affinity interactions observed in lysate is an open question.

In contrast to the relatively poor correlation for Ca^{2+}-CaM observed in Fig. 3a, a much better correlation is noted for the Ca^{2+}-CaM-smMLCK(p) complex, Fig. 3b. The excellent agreement in Fig. 3b provides a validation of the

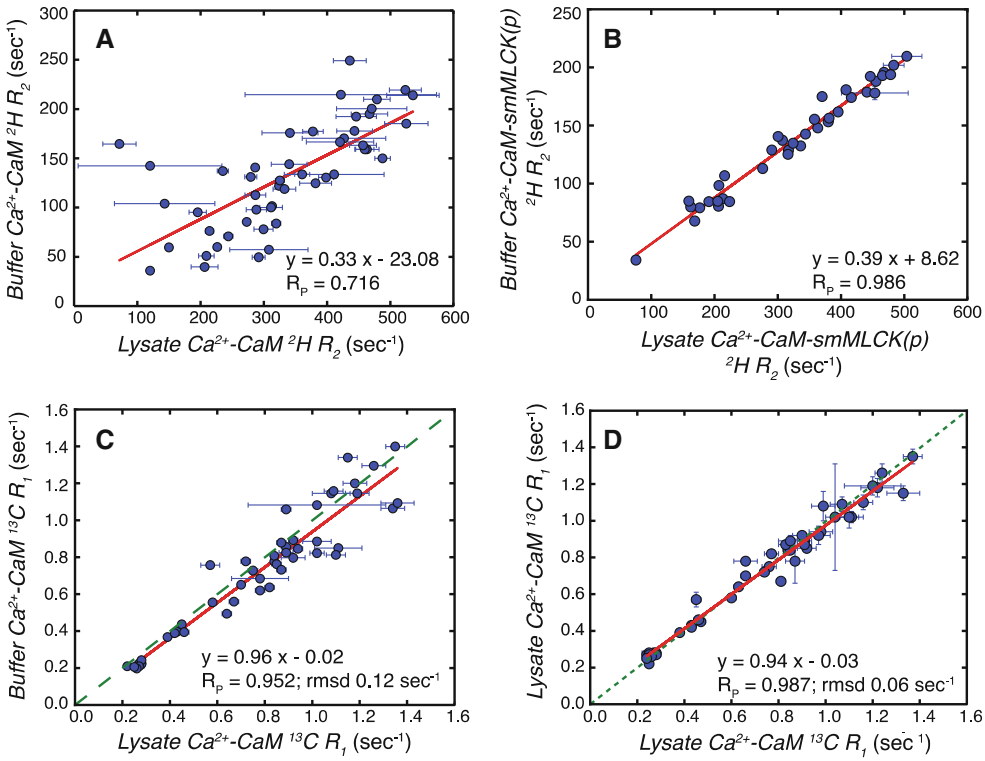

Fig. 3 Correlation plots of ^{2}H R_2 relaxation rates for **a** Ca^{2+}-CaM or **b** Ca^{2+}-CaM-smMLCK(p) measured in buffer (y-axis) or 100 g/L *E. coli* lysate (x-axis), 18 °C, 14.1 T. The best-fit line is shown in *red*, along with the corresponding equation and Pearson's correlation coefficient (R_P), in the lower right hand corner. Larger errors in the Lysate Ca^{2+}-CaM measurements are the result of peak broadening due to ms time-scale exchange (see Fig 1b, c). Correlation plots of ^{13}C R_1 relaxation rates for Ca^{2+}-CaM in buffer versus 100 g/L *E. coli* lysate **c** or duplicate measurements in lysate **d**. The *green dashed line* is y = x, while the best-fit line is in *red*. The pair-wise rmsd of experimental values, along with R_p and the equation of the best-fit line are in the lower right corner

^{2}H relaxation methodology. Moreover, it is consistent with a lack of interactions between Ca^{2+}-CaM-smMLCK(p) and lysate, as expected, since (1) no changes in chemical shifts between buffer and lysate samples were observed in this case (Fig. 1a) and (2) the significant contribution to transverse relaxation for Ca^{2+}-CaM in lysate, reflecting an exchange process with *E. coli* peptides/proteins, disappears upon addition of saturating amounts of smMLCK(p) (Fig. 1b). We have also measured ^{13}C R_1 values for Ca^{2+}-CaM in both buffer and lysate, Fig. 3c, and the correlation observed is poorer than expected based on experimental error. That this is the case can be seen from repeat measurements of R_1 values for Ca^{2+}-CaM in lysate, Fig. 3d, where the pair-wise rmsd is a factor of two smaller than for the correlation of R_1 rates measured on buffer and lystate samples (Fig. 3c). Simulations establish that for CaM in buffer ($\tau_C \sim 15$ ns) and lysate ($\tau_C \sim 40$ ns) ^{13}C R_1 rates report almost exclusively on the timescale of motion of the methyl threefold axis (τ_e) and are relatively insensitive to S^2. Thus, our results provide strong evidence that binding of even low affinity partners modulates methyl τ_e values in CaM.

Comparison of Ca^{2+}-CaM in different lysates

To this point our study has focused on *E. coli* lysate as a mimic of the *in-cell* environment. We have shown here and in a related publication (Latham and Kay 2012) that Ca^{2+}-CaM transiently interacts with non-cognate binding partners, leading to changes in chemical shifts, large contributions to ^{1}H and ^{13}C transverse relaxation rates from chemical exchange between bound and free forms of the protein and changes in ^{2}H R_2 and ^{13}C R_1 values. It is of interest to consider what happens when eukaryotic *S. cerevisiae* lysate is substituted for the *E. coli* version because CaM is a eukaryotic protein and there are thus many cognate and high affinity binding partners, involved in CaM mediated Ca^{2+} signaling, that become available in this new environment (O'Neil and DeGrado 1990; Hoeflich and Ikura 2002; Yamniuk and Vogel 2004).

Figure 4 shows a comparison of 2D ^{13}C–^{1}H spectra of 50 μM Ca^{2+}-CaM in 100 g/L eukaryotic *S. cerevisiae* and bacterial *E. coli* lysates. At the relatively low concentrations of protein used all of the Ca^{2+}-CaM in the yeast lysate is sequestered in a large number of high affinity complexes in slow exchange, resulting in a severe dilution of NMR signals. By contrast, we have shown that Ca^{2+}-CaM in *E. coli* lysate exchanges rapidly between low affinity complexes to give a single average signal for each methyl site, and hence a much higher quality spectrum than for the yeast lysate. Only for concentrations of Ca^{2+}-CaM that exceed ~0.5 mM, when the CaM specific interactions are saturated, does the spectrum in 100 g/L yeast lysate approximate the quality observed in Fig. 1c (data not shown). In order to establish that different sample viscosities are not responsible for the

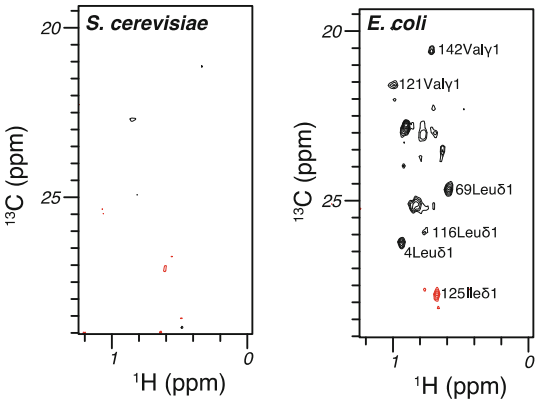

Fig. 4 Leu/Val region of ^{13}C–^{1}H correlation spectra of 50 μM Ca^{2+}-CaM in 100 g/L *S. cerevisiae* (*left*) or *E. coli* (*right*). Spectra were recorded at 14.1 T and 18 °C with a previously described pulse sequence for measuring the ^{2}H R_2 relaxation rates and $T = 0$ (Tugarinov et al. 2005). The correlation in *red* is aliased

differences in the quality of the spectra in Fig. 4, we have measured the translational diffusion coefficients for Ca^{2+}-CaM-smMLCK(p) in both lysates utilizing a 1D ^{2}H,^{13}C-edited pulse field gradient based experiment. NMR spectra of Ca^{2+}-CaM-smMLCK(p) in the two environments are identical indicating that CaM in the smMLCK(p) bound state does not interact strongly with either lysate; hence, the relative diffusion constants are expected to provide an indication of how viscosities of the media differ. Diffusion constant values of $(2.69 \pm 0.45) \times 10^{-7}$ cm^2 s^{-1} (yeast) and $(2.23 \pm 0.46) \times 10^{-7}$ cm^2 s^{-1} (*E. coli*) confirm that indeed the absence of resonances in the *S. cerevisiae* lysate is due to specific binding to yeast proteins and not the result of increased viscosity.

Concluding remarks

We have presented a solution based NMR study of U-[^{2}H,^{15}N], Ileδ1-[^{13}CHD$_2$], Leuδ,Valγ-[^{13}CHD$_2$], Metε-[^{13}CHD$_2$] labeled Ca^{2+}-CaM to probe interactions in the heterogeneous cell-like environment of *E. coli* lysate. Analysis of chemical shift data as a function of added lystate establishes that Ca^{2+}-CaM interacts transiently and weakly with non-cognate *E. coli* peptide/proteins; such interactions are confirmed on the basis of CPMG relaxation dispersion and ^{2}H R_2, ^{13}C R_1 experiments. Analysis of the titration data provides a lower limit on K_D (~0.2 mM) as well as an average value for $C_{Lys,1/2}$, 26 g/L, that translates into 1.63 mg *E. coli* lysate/mg of CaM to achieve a half bound state. Differences in spectra of Ca^{2+}-CaM in *E. coli* and yeast lysates can be rationalized in terms of the rapid interconversion between different transient complexes that leads to averaging of chemical shifts (*E. coli*) versus much stronger interactions with cognate proteins that dilutes the NMR signal (yeast). Further, this study highlights the utility of methyl group probes in protein studies, including those in complex, heterogeneous milieus such as that of an in-cell like environment.

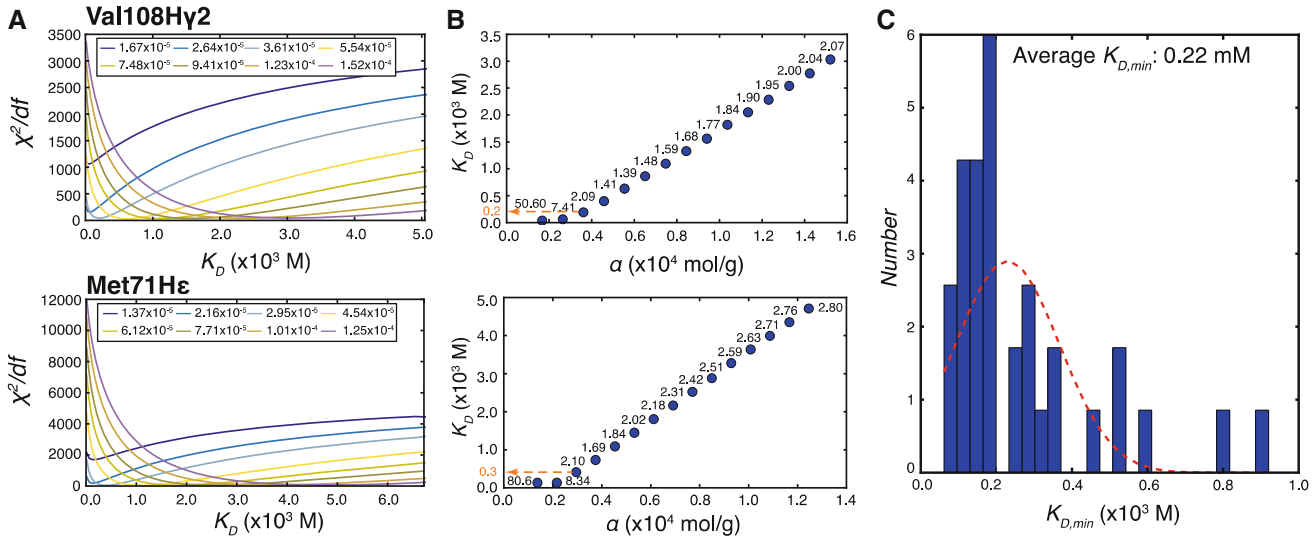

Fig. 5 **a** 1D χ^2 grid searches as a function of K_D for a number of α values (listed at the top of each graph). The grid searches were performed in the vicinity of the best fit (α, K_D) values, corresponding to (5.070e–05 mol/g, 5.15e–04 M) and (3.355e–05 mol/g, 5.25e–04 M) for Val108Hγ2 and Met71Hε, respectively. **b** Linear relationship between K_D and α for the residues in **a**. The reduced χ^2 that is obtained when the listed (α, K_D) pairs are used is given above (or next to) each point. The *orange dashed line* denotes $K_{D,min}$. **c** Histogram of $K_{D,min}$ values. The red dashed line is the Gaussian profile generated with the trimmed mean and standard deviation of the distribution. The trimmed mean was calculated by discarding values outside 2 times the standard deviation of the mean

Acknowledgments The authors thank Professor Mistu Ikura (Ontario Cancer Institute) for the gift of a CaM plasmid and assignments for Ca^{2+}-CaM and Dr. John Rubinstein (Hospital for Sick Children) for providing laboratory space. M. P. L. acknowledges support in the form of post-doctoral fellowships from the National Science Foundation (OISE-0853108) and the Canadian Institutes of Health Research (CIHR) Training Grant in Protein Folding and Disease. This work was supported by a grant from the CIHR. L. E. K. holds a Canada Research Chair in Biochemistry.

Appendix: Fits of titration curves yield a range of (α, K_D) values

As described in the text each of the titration profiles was fit to Eq. (2) to generate best fit values for (α, K_D). We have performed grid searches as a function of K_D for a number of α values in the vicinity of the best fit α value and calculated χ^2/df. Figure 5A shows results for a pair of residues, Val108Hγ2 and Met71Hε. It is clear that there is a range of (α, K_D) that fit the data essentially equally well and that a minimum K_D value can be approximated. Notably, each (α, K_D) pair that produces a low residual lies on the line given by Eq. (5), as shown in Fig. 5B, with the χ^2/df indicated for each point. A lower bound for K_D ($K_{D,min}$) can be read off of each plot, corresponding to the point where the curve deviates from linearity. Figure 5C plots a histogram of $K_{D,min}$ values, showing the range obtained.

References

Baldwin AJ, Religa TL, Hansen DF, Bouvignies G, Kay LE (2010) (13)CHD(2) methyl group probes of millisecond time scale exchange in proteins by (1)H relaxation dispersion: an application to proteasome gating residue dynamics. J Am Chem Soc 132:10992–10995. doi:10.1021/ja104578n

Campbell ID, Dwek RA (1984) Biological spectroscopy, 1st edn. Benjamin-Cummings Publishing Co., Menlo Park, p 422

Carr H, Purcell E (1954) Effects of diffusion on free precession in nuclear magnetic resonance experiments. Phys Rev 94:630–638. doi:10.1103/PhysRev.94.630

Delaglio F, Grzesiek S, Vuister GW, Zhu G, Pfeifer J, Bax A (1995) NMRPipe: a multidimensional spectral processing system based on UNIX pipes. J Biomol NMR 6:277–293

Fulton AB (1982) How crowded is the cytoplasm? Cell 30:345–347

Hoeflich KP, Ikura M (2002) Calmodulin in action: diversity in target recognition and activation mechanisms. Cell 108:739–742

Hong J, Gierasch LM (2010) Macromolecular crowding remodels the energy landscape of a protein by favoring a more compact unfolded state. J Am Chem Soc 132:10445–10452. doi:10.1021/ja103166y

Ikura M, Clore GM, Gronenborn AM, Zhu G, Klee CB, Bax A (1992) Solution structure of a calmodulin-target peptide complex by multidimensional NMR. Science 256:632–638

Ishima R, Torchia D (2000) Protein dynamics from NMR. Nat Struct Biol 7:740–743. doi:10.1038/78963

Johnson PE, Tomme P, Joshi MD, McIntosh LP (1996) Interaction of soluble cellooligosaccharides with the N-terminal cellulose-binding domain of Cellulomonas fimi CenC 2. NMR and ultraviolet absorption spectroscopy. Biochemistry 35:13895–13906. doi:10.1021/bi961186a

Latham MP, Kay LE (2012) Is buffer a good proxy for a crowded cell-like environment? A comparative nmr study of calmodulin side-chain dynamics in buffer and E. coli Lysate. PLoS ONE 7:e48226. doi:10.1371/journal.pone.0048226

Lee AL, Kinnear SA, Wand AJ (2000) Redistribution and loss of side chain entropy upon formation of a calmodulin-peptide complex. Nat Struct Biol 7:72–77. doi:10.1038/71280

Li C, Pielak GJ (2009) Using NMR to distinguish viscosity effects from nonspecific protein binding under crowded conditions. J Am Chem Soc 131:1368–1369. doi:10.1021/ja808428d

Meiboom S, Gill D (1958) Modified Spin-Echo method for measuring nuclear relaxation times. Rev Sci Instrum 29:688. doi:10.1063/1.1716296

Miklos AC, Li C, Sharaf NG, Pielak GJ (2010) Volume exclusion and soft interaction effects on protein stability under crowded conditions. Biochemistry 49:6984–6991. doi:10.1021/bi100727y

Miklos AC, Sarkar M, Wang Y, Pielak GJ (2011) Protein crowding tunes protein stability. J Am Chem Soc 133:7116–7120. doi:10.1021/ja200067p

Mittermaier AK, Kay LE (2006) New tools provide new insights in NMR studies of protein dynamics. Science 312:224–228. doi:10.1126/science.1124964

Muhandiram DR, Yamazaki T, Sykes BD, Kay LE (1995) Measurement of 2H T1 and T1ρ relaxation times in uniformly 13C-labeled and fractionally 2H-labeled proteins in solution. J Am Chem Soc 117:11536–11544. doi:10.1021/ja00151a018

Neidhardt FC (1987) *Escherichia coli* and *Salmonella typhimurium*. Am Soc Microbiol 1:3–6

O'Neil KT, DeGrado WF (1990) How calmodulin binds its targets: sequence independent recognition of amphiphilic alpha-helices. Trends Biochem Sci 15:59–64

Palmer AG, Kroenke CD, Loria JP (2001) Nuclear magnetic resonance methods for quantifying microsecond-to-millisecond motions in biological macromolecules. Methods Enzymol 339:204–238

Press WH, Flannery BP, Teukolsky SA, Vetterling WT (1992) Numerical Recipes in C: the art of scientific computing, 2nd edn. 994

Reckel S, Hansel R, Lohr F, Dötsch V (2007) In-cell NMR spectroscopy. Prog NMR Spectr 51:91–101. doi:10.1016/j.pnmrs.2007.02.002

Sakai T, Tochio H, Tenno T, Ito Y, Kokubo T, Hiroaki H, Shirakawa M (2006) In-cell NMR spectroscopy of proteins inside Xenopus laevis oocytes. J Biomol NMR 36:179–188. doi:10.1007/s10858-006-9079-9

Selenko P, Serber Z, Gadea B, Ruderman J, Wagner G (2006) Quantitative NMR analysis of the protein G B1 domain in Xenopus laevis egg extracts and intact oocytes. Proc Natl Acad Sci USA 103:11904–11909. doi:10.1073/pnas.0604667103

Serber Z, Keatinge-Claya T, Ledwidge R, Kelly AE, Miller SM, Dötsch V (2001) High-resolution macromolecular NMR spectroscopy inside living cells. J Am Chem Soc 123:2446–2447

Shaka A, Reeler J, Frenkiel T, Freeman R (1983) An improved sequence for broadband decoupling: WALTZ-16. J Magn Reson 52:335–338

Siivari K, Zhang M, Palmer AG, Vogel HJ (1995) NMR studies of the methionine methyl groups in calmodulin. FEBS Lett 366:104–108

Tugarinov V, Kay LE (2005) Quantitative 13C and 2H NMR relaxation studies of the 723-residue enzyme malate synthase G reveal a dynamic binding interface. Biochemistry 44:15970–15977. doi:10.1021/bi0519809

Tugarinov V, Ollerenshaw JE, Kay LE (2005) Probing side-chain dynamics in high molecular weight proteins by deuterium NMR

spin relaxation: an application to an 82-kDa enzyme. J Am Chem Soc 127:8214–8225. doi:10.1021/ja0508830

Tugarinov V, Kanelis V, Kay LE (2006) Isotope labeling strategies for the study of high-molecular-weight proteins by solution NMR spectroscopy. Nat Protoc 1:749–754. doi:10.1038/nprot.2006.101

Vranken WF, Boucher W, Stevens TJ, Fogh RH et al (2005) The CCPN data model for NMR spectroscopy: development of a software pipeline. Proteins 59:687–696. doi:10.1002/prot.20449

Wang Q, Zhuravleva A, Gierasch LM (2011) Exploring weak, transient protein–protein interactions in crowded in vivo environments by in-cell nuclear magnetic resonance spectroscopy. Biochemistry 50:9225–9236. doi:10.1021/bi201287e

Yamniuk AP, Vogel HJ (2004) Calmodulin's flexibility allows for promiscuity in its interactions with target proteins and peptides. Mol Biotechnol 27:33–57. doi:10.1385/MB:27:1:33

Zuiderweg ERP (2002) Mapping protein–protein interactions in solution by nmr spectroscopy. Biochemistry 41:1–7. doi:10.1021/bi011870b